

Theoretical studies on reaction mechanism of H₂ with COS

Riguang Zhang · Lixia Ling · Baojun Wang

Received: 23 November 2009 / Accepted: 29 January 2010 / Published online: 17 March 2010
© Springer-Verlag 2010

Abstract The reaction mechanisms of H₂ with OCS have been investigated theoretically by using density function theory method. Three possible pathways leading to major products CO and H₂S, as well as two possible pathways leading to by-product CH₄ have been proposed and discussed. For these reaction pathways, the structure parameters, vibrational frequencies and energies for each stationary point have been calculated, and the corresponding reaction mechanism has been given by the potential energy surface, which is drawn according to the relative energies. The calculated results show that the corresponding major products CO and H₂S as well as by-product CH₄ are in agreement with experimental findings, which provided a new illustration and guidance for the reaction of H₂ with OCS.

Keywords COS · Density functional theory · H₂ · Reaction mechanism

Introduction

Carbonyl sulfide (OCS) commonly exists in coke oven gas, coal making gas, natural gas, petroleum refining exhaust gases, the flue gas, vehicle exhaust and Claus tail gases [1–4]. In the processes of manufacturing, OCS not only leads to corrosion of the reaction equipments but also results in the deactivation of catalysts [4, 5]. To avoid equipment corrosion and catalyst poisoning, the main

technologies including catalytic hydrolysis, oxidation conversion, and hydrogenation conversion, etc. [6, 7] have been used for the removal of OCS. Among these methods, hydrogenation conversion of OCS to CO and H₂S was the most principal technology. Especially, for the removal of COS from the hydrogen-rich gases, hydrogenation conversion shows very high conversion efficiency for OCS and adequately makes use of hydrogen existing in hydrogen-rich gases [8, 9]. However, a major challenge associated with hydrogenation conversion of OCS is the formation of undesirable by-product CH₄ [6, 8]. Up to now, to the best of our knowledge, few theoretical explanations for this experimental fact were reported, and the reasons why CO and H₂S are the main products and CH₄ is a by-product are not illustrated. Therefore, it is of great significance to study the reaction mechanism of OCS with H₂. For a detailed understanding of the reaction mechanism of OCS hydrogenation conversion, experimental information is however not always sufficient and accompanying theoretical calculations can be helpful to clarify some questions. Quantum chemical methods have become new tools for determining reaction mechanisms. With recent developments, density functional theory (DFT) is capable of providing qualitative and quantitative insights into reaction mechanism [10]. Nowadays, literature [11] has reported the similar reaction of H with OCS, the calculations results provide the first set of structural data that detail the reaction mechanisms for H with OCS going to SH and CO or OH and CS, which substantiate experimental hypotheses of the existence of stable, four-body reaction intermediates, as well as tight four-body transition states leading to products [12]. Zhang et al. [13] have investigated the reaction of CN radical with OCS by using ab initio MO method, six possible product channels have been discussed, the calculated results show that the

R. Zhang · L. Ling · B. Wang (✉)
Key Laboratory of Coal Science and Technology
of Ministry of Education and Shanxi Province,
Taiyuan University of Technology,
Taiyuan 030024, China
e-mail: wangbaojun@tyut.edu.cn

reaction channel of producing CO and NCS is the main reaction channel.

In our studies, we will focus mostly on the theoretical studies about the reaction mechanism of H₂ with OCS by using DFT calculations, which will be helpful to deeply understand the mechanism in the views of quantum chemistry. Calculated results are expected to explain the experimental findings and give a new illustration and guidance for the reaction of H₂ with OCS that could not be reached experimentally under the considered conditions.

Computational methods

The structures of all the stationary points (reactants, intermediates, transition states, and products) involved in the reaction pathways of H₂ with COS were fully optimized at the level of the general gradient approximation (GAA) using BLYP functional [14, 15]. The double-numeric quality basis set with polarization functions (DNP) was used here. The size of the DNP basis set is comparable to Gaussian 6-31G**, but the DNP is more accurate than the Gaussian basis set of the same size. Moreover, this basis set is known to produce a small basis set super position error (BSSE) [16]. And the zero-point energy (ZPE) of these stationary points was determined. The reaction pathways have been examined by performing TS confirmation on most of the transition state structures to confirm that they lead to the desired reactants and products [17]. All calculations were performed with Dmol³ using the Materials studio program package on Pentium D PC [18, 19].

Results and discussion

Evaluation of the computational accuracy

To evaluate the reliability of the chosen level of theory, we calculated the bond dissociation energies (BDE) for several

species involved in the reaction of H₂ with OCS using several popular functionals in Dmol³ program: GGA-BLYP, GGA-PW91 and LDA-PWC. The relevant results were listed in Table 1, where the available experimental and calculated values were also presented for comparison.

As presented in Table 1, by comparing these theoretical values with experimental findings, we found that BLYP functional gave relatively smaller absolute errors than PW91 and PWC functionals. Therefore, the calculated results from GGA-BLYP can be considered satisfactory, considering our main goals in the present work are the examination of the detailed reaction mechanism and the calculation of the relative energies of the species involved, not the calculation of accurate bond energies.

For the OCS molecule, we calculated its properties, including the geometric structures, vibrational frequencies, as well as C–O and C–S bond dissociation energies. The relevant results are shown in Tables 1 and 2, respectively. Clearly, the chosen level of theory reproduces all properties of the OCS molecule well. According to above evaluation, we are confident in the ability of the chosen level of theory to describe the features of the potential energy surface of the reaction H₂ with OCS.

Reaction mechanism

In the process of H₂ and OCS approaching each other, various possible products can be formed when different atoms of the two reactant molecules interact in the reaction. Five possible pathways have been proposed for the reaction of H₂ with OCS, and it can be summarized as Scheme 1 describes.

The optimized geometries for the reactants, intermediates, transition states, products and their atomic number along the reaction pathways are shown schematically in Fig. 1. The corresponding total energies, zero-point energies, relative energies, barrier height together with imaginary frequency corresponding to transition states are listed in Table 3. The overall energetic profile for the

Table 1 Theoretical and experimental bond dissociation energies (kJ·mol⁻¹)

Species	Calculated				Experimental
	GGA-BLYP	GGA-PW91	LDA-PWC	GGA-BLYP ^a	
OC–S	318.6	361.8	322.1	316.1	308.4 ^b
O–CS	689.6	746.7	697.9	687.8	664.9±0.85 ^c
C–S	701.0	725.9	686.7	699.6	712.2±0.85 ^d
O–C	1079.3	1110.8	1062.5	1071.1	1076.4±0.67 ^b
H ₃ C–H	439.1	438.5	458.8	—	439.9±0.40 ^b
HS–H	384.1	352.9	349.4	—	381.4±0.50 ^b
HO–H	484.1	493.9	478.5	—	497.1±0.29 ^b
H–H	446.4	429.3	454.0	—	435.8 ^b

^a Ref. [20] ^b Ref. [21] ^c Ref. [22]

^d Ref. [23]

Table 2 Theoretical and experimental properties for the ground state OCS molecule^a

	R _{C-S}	R _{C-O}	ω_1	ω_2	ω_3
Calculated GGA-BLYP	1.579	1.176	2030	846	505
Experimental ^b	1.561	1.156	2072	866	520

^a The symbols R and ω denote the bond length (\AA) and vibrational frequencies (cm^{-1}), respectively.

^b Ref. [24].

reaction of H_2 with OCS leading to CO and H_2S is presented in Fig. 2. Zero-point energies have been included in all cited energies.

R1~R8 is the reactant-like intermediate, in which two reactant molecules interact with each other by van der Waals force, and their geometries remain almost the same with the corresponding free molecules. P1~P5 is the product-like intermediate, in which the products interact in a similar way. R1~R8 are more stable than the original reactants.

Firstly, along reaction pathways of H_2 with OCS leading to products CO and H_2S , as shown in Scheme 1 and Fig. 1, it can be seen that when the H_2 and S atom of OCS interacts in Path 1 through TS1, In TS1, the breaking C2–S3 bond is 1.103 \AA longer than that of OCS, and the O1C2S3 angle changes from 180.00° in OCS to 129.63°. The original linear OCS molecule is distorted. The forming H4–S3 and H5–S3 bond is 1.608 \AA and 1.853 \AA , respectively. The O1–C2 bond shortens from 1.176 to 1.149 \AA . The barrier height of TS1 relative to R1 is 363.0 $\text{kJ}\cdot\text{mol}^{-1}$.

When the H_2 attack the end S atom and center C atom of OCS in Path 2, R2 is converted to IM1 via a four-center TS2, in which H4 and H5 of H_2 interacts with C2 and S3 of

OCS to form a four-center ring among C2–S3–H5–H4. And the H4–H5 and C2–S3 bonds elongate from 0.747 to 1.023 \AA and from 1.580 to 1.695 \AA , respectively. The C2–H4 and S3–H5 distances shorten from 3.449 to 1.498 \AA and from 3.621 to 1.746 \AA , respectively. Moreover, the original linear OCS molecule is severely distorted. The O1C2S3 angle changes from 179.88° in R2 to 145.68°. TS2 is 283.6 $\text{kJ}\cdot\text{mol}^{-1}$ less stable compared to R2. IM1 is further converted to P2 via a concerted transition state TS3 of C2–S3 bond cleavage and 1, 2-hydrogen migration from C2 to S3. TS3 is located to be 222.4 $\text{kJ}\cdot\text{mol}^{-1}$ above the reactants and 193.7 $\text{kJ}\cdot\text{mol}^{-1}$ above forward intermediate IM1. So the rate determining step is R2→IM1 via TS2 in Path 2 with an activation barrier of 283.6 $\text{kJ}\cdot\text{mol}^{-1}$.

Then, besides the above-mentioned two pathways, another possible reaction Path 3 were found as presented in Scheme 1, when the H_2 attack the end S and O atom of OCS, which results in the reactant-like intermediate R3. Then, R3 is converted to IM2 via a five-center TS4, in which H4 and H5 of H_2 interacts with O1 and S3 in OCS to form a five-center ring among O1–C2–S3–H5–H4. The O1C2S3 angle changes from 179.79° in R3 to 119.42°. TS4 is 293.3 $\text{kJ}\cdot\text{mol}^{-1}$ higher in energy than R3. IM2 is much higher in total energy than IM1, so IM2 is not stable, and quickly converted to P3 leading to products CO and H_2S via a concerted transition state TS5 of C2–S3 bond cleavage and 1,3-hydrogen migration from O1 to S3. TS5 is predicated to be 76.9 $\text{kJ}\cdot\text{mol}^{-1}$ higher in energy than forward intermediate IM2. Therefore, R3→IM2 via TS4 is the rate determining step of Path 3 with an activation barrier of 293.3 $\text{kJ}\cdot\text{mol}^{-1}$.

From Fig. 2, it can be seen that the first reaction step proceeding via TS1, TS2 and TS4 is the rate determining step in Paths 1~3, and the corresponding activation barriers are 363.0, 283.6 and 293.3 $\text{kJ}\cdot\text{mol}^{-1}$ relative to the reactant-like intermediate, respectively. In view of activation barriers, Path 1 is the most unfavorable pathway. The energy barrier of Path 2 is the lowest. Obviously, Path 2 is the main reaction pathways for the initial reaction of COS and H_2 , which result in the products CO and H_2S . It can be seen that the activation barriers of Paths 2 and 3 are close; we guess that Paths 2 and 3 may be two-parallel reaction pathways resulting in the formation of CO and H_2S . So the corresponding rate constants would be discussed in “The rate constant for the reaction paths 2 and 3” below.

Next, along the reaction pathways of H_2 with OCS leading to the formation of by-product CH_4 , as shown in Scheme 1. R2→IM1 in Path 4 is similar to Path 2. Besides 1, 2-hydrogen migration for IM1, H_2 can also react with IM1 to form IM4 via H_2 addition to C=O bond. The corresponding transition state is TS6, whose barrier height is 335.9 $\text{kJ}\cdot\text{mol}^{-1}$ seen from Table 3.

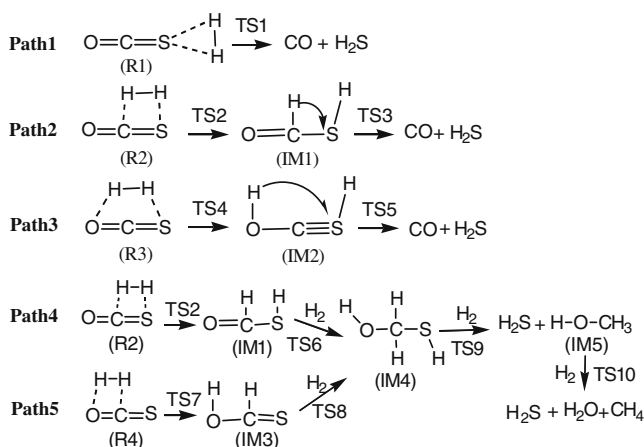
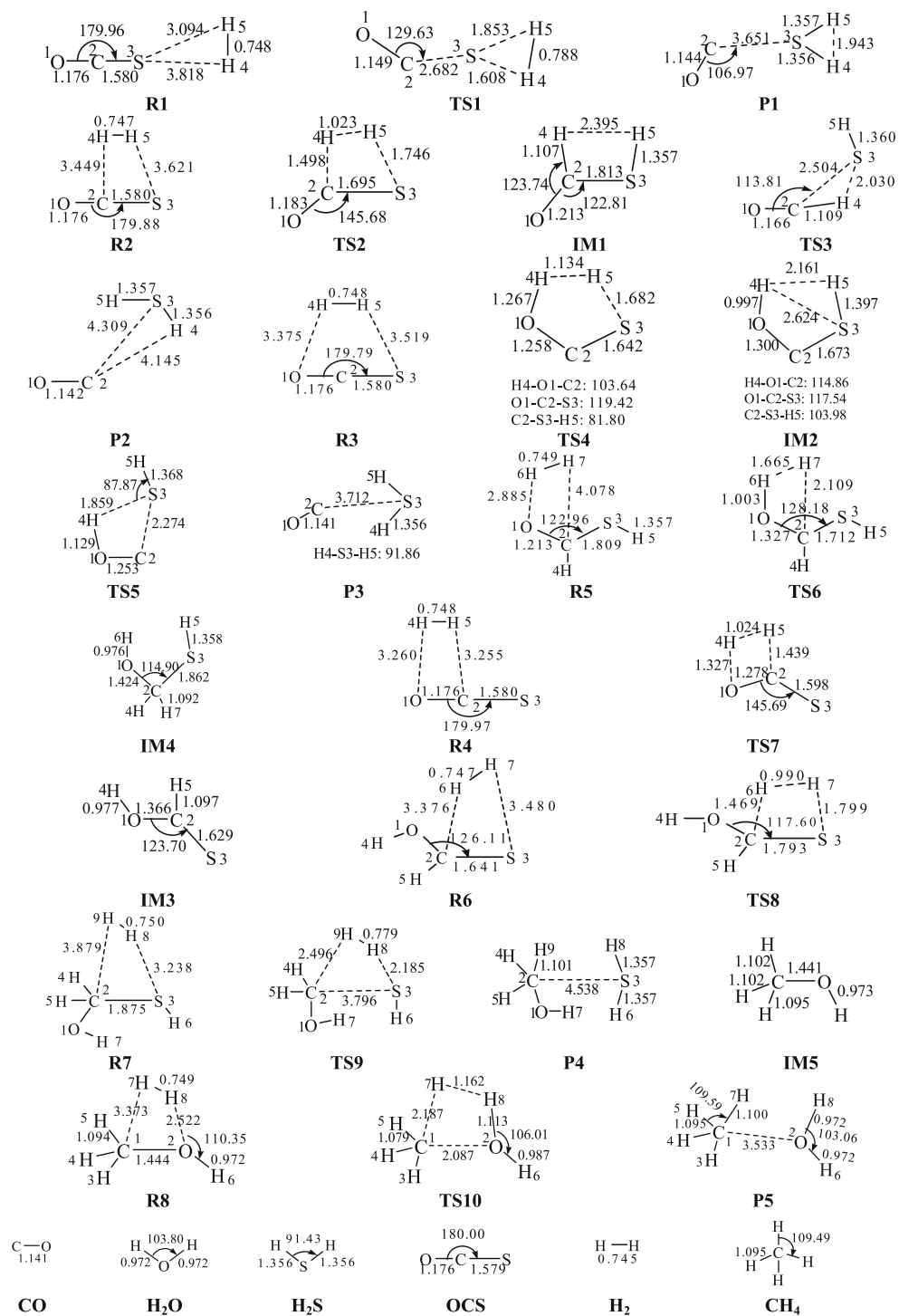
**Scheme 1** The proposed mechanisms of H_2 reacting with OCS leading to products CO, H_2S , H_2O and CH_4

Fig. 1 The optimized geometries for various species involved in the reaction of H₂ with OCS (IM—intermediate, TS—transition state). Bond lengths are in angstroms and angles in degree



When the H₂ attacks the end O atom and center C atom of OCS in Path 5, R4 is converted to IM3 *via* a four-center TS7, in which H4 and H5 of H₂ interacts with O1 and C2 of OCS to form a four-center ring among O1–C2–H5–H4, the H4–H5 and O1–C2 bonds elongate from 0.748 to 1.024 Å and from 1.176 to 1.278 Å, respectively. The O1–H4 and C2–H5 distances shorten from 3.260 to 1.327 Å and from 3.255 to 1.439 Å, respectively. The original linear OCS molecule is

also distorted, and the O1C2S3 angle changes from 179.97° in R4 to 145.69°. The barrier height of TS7 relative to R4 is 326.3 kJ·mol⁻¹. IM3 further interact with H₂ to yield R6, R6 leads to the formation of IM4 *via* TS8. TS8 is 256.5 kJ·mol⁻¹ higher than R6. It can be seen that the barrier of C=O addition with H₂ is higher than that of C=S addition, which may be because the BDE of C=O bond is stronger than that of C=S bond, which is in agreement with the literature [21, 22].

Table 3 Total and relative energies for every stationary point of different species, barrier height and partial vibrational frequencies involved in various reaction pathways

	E_T (hartree)	E_0 (hartree)	E_c (hartree)	E_{rel} (kJ·mol $^{-1}$)	E_{bh} (kJ·mol $^{-1}$)	IF (cm $^{-1}$)
COS	-511.59832	0.00883	-511.58949			
H ₂	-1.16663	0.01011	-1.15652			
COS+H ₂	-512.76495	0.01894	-512.74601	0.00		
R1	-512.76798	0.02025	-512.74773	-4.5		
TS1	-512.62665	0.01719	-512.60945	358.5	363.0	-780.0i
P1	-512.75082	0.02064	-512.73018	41.6		
R2	-512.76768	0.01963	-512.74805	-5.4		
TS2	-512.65946	0.01943	-512.64004	278.2	283.6	-2028.8i
IM1	-512.76210	0.02703	-512.73507	28.7		
TS3	-512.68233	0.02103	-512.66130	222.4	193.7	-1204.6i
P2	-512.75111	0.02104	-512.73007	41.9		
R3	-512.76763	0.01957	-512.74807	-5.4		
TS4	-512.65676	0.02042	-512.63634	287.9	293.3	-1607.9i
IM2	-512.68414	0.02549	-512.65864	229.4		
TS5	-512.64964	0.02030	-512.62934	306.3	76.9	-1206.7i
P3	-512.75036	0.02093	-512.72943	43.5		
CO+H ₂ S	-512.74672	0.02005	-512.72667	50.8		
CO	-113.34490	0.00478	-113.34012			
H ₂ S	-399.40182	0.01527	-399.38655			
COS+H ₂	-512.76495	0.01894	-512.74601	0.00		
R2	-512.76768	0.01963	-512.74805	-5.4		
TS2	-512.65946	0.01943	-512.64004	278.2	283.6	-2028.8i
IM1	-512.76210	0.02703	-512.73507	28.7		
IM1+H ₂	-513.92873	0.03714	-513.89159	0.0		
R5	-513.93184	0.03875	-513.89309	-3.9		
TS6	-513.80684	0.04171	-513.76513	332.0	335.9	-806.4i
IM4	-513.94872	0.05014	-513.89859	-18.4		
COS+H ₂	-512.76495	0.01894	-512.74601	0.00		
R4	-512.76763	0.02004	-512.74758	-4.1		
TS7	-512.64298	0.01968	-512.62330	322.2	326.3	-2276.6i
IM3	-512.74687	0.03052	-512.71636	77.9		
IM3+H ₂	-513.91350	0.04062	-513.87288	0.0		
R6	-513.92465	0.04168	-513.88296	-26.5		
TS8	-513.82774	0.04248	-513.78526	230.0	256.5	-1880.8i
IM4	-513.94872	0.05014	-513.89859	-67.5		
IM4+H ₂	-515.11535	0.06024	-515.05511	0.0		
R7	-515.11724	0.06179	-515.05545	-0.9		
TS9	-515.01649	0.05818	-514.95831	254.2	255.1	-469.0i
P4	-515.13981	0.06592	-515.07390	-49.3		
IM5+H ₂ S	-515.13556	0.06550	-515.07006	-39.2		
IM5	-115.73374	0.05023	-115.68351			
IM5+H ₂	-116.90037	0.06033	-116.84003	0.0		
R8	-116.90297	0.06275	-116.84022	-0.5		
TS10	-116.77277	0.05813	-116.71464	329.2	329.7	-1324.4i
P5	-116.94719	0.06609	-116.88110	-107.8		
H ₂ O+CH ₄	-116.94520	0.06520	-116.88000	-104.9		
H ₂ O	-76.44643	0.02118	-76.42525			
CH ₄	-40.49877	0.04402	-40.45475			

E_T —Total energy, E_0 —Zero-point energy, E_c —Corrected energy for Zero-point energy, E_{rel} —Relative energy (with OCS+H₂ as reference in pathway leading to CO and H₂S, IM1 and IM3, with X+H₂ as reference in pathway leading to other species), E_{bh} —Barrier height, IF —Imaginary frequency

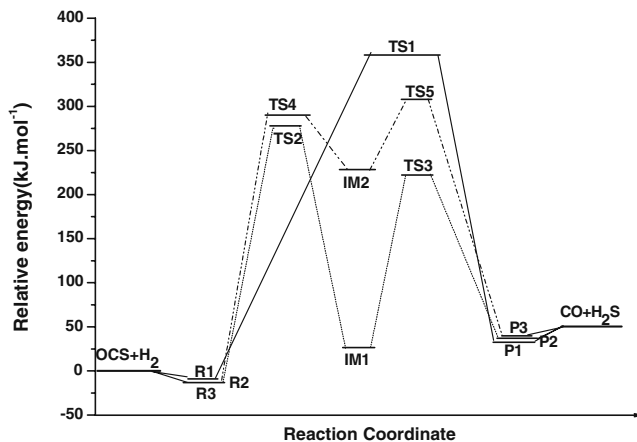


Fig. 2 Schematic energy profiles for the reaction of H_2 with OCS leading to CO and H_2S along the three possible pathways described in Scheme 1

Starting from the intermediate IM4, as shown in Fig. 1, the bond length for O1–C2 is 1.424 Å and 1.862 Å for C2–S3 bond in IM4. The comparison between the BDE of S–C bond in HS–CH₃ ($312.5 \pm 4.2 \text{ kJ}\cdot\text{mol}^{-1}$) [25] and O–C bond in HO–CH₃ ($384.93 \pm 0.71 \text{ kJ}\cdot\text{mol}^{-1}$) [26] in experiment suggests that the breaking O1–C2 bond is strong and the breaking S3–C2 bond is weak in IM4, and the corresponding barrier of O1–C2 bond cleavage *via* H_2 reaction is higher than that of C2–S3 bond cleavage. So H_2 easily attacks the end S and center C of IM4 leading to reactant-like intermediate R7, R7 is converted to P4 *via* a concerted four-center transition state TS9 of H8–H9 and C2–S3 bond cleavage with a barrier height of 255.1 $\text{kJ}\cdot\text{mol}^{-1}$. P4, the complex of H_2S and IM5, forms the products of H_2S and IM5. Then, IM5 further interact with H_2 to yield intermediate R8, R8 starts with a concerted H7–H8 and C1–O2 bond cleavage at transition state TS10, which was found to be 329.7 $\text{kJ}\cdot\text{mol}^{-1}$ higher in energy than R8. This is significantly lower than the BDE of C–O bond in HO–CH₃, which may be attributed to the synchronous effect of H7–H8 bond cleavage of H_2 and C1–O2 bond cleavage. Then, P6 can form by-products CH₄.

After this, according to the above discussion about the reaction mechanisms of H_2 with OCS. It is concluded that the determining step of Paths 4 and 5 is that *via* TS6 and TS10, respectively. And the corresponding activation

barrier are 335.9 and 329.7 $\text{kJ}\cdot\text{mol}^{-1}$, respectively. At the same time, in the reaction of H_2 with OCS leading to products CO and H_2S , the corresponding activation barriers of two possible reaction pathways *via* TS2 and TS4 are 283.6 and 293.3 $\text{kJ}\cdot\text{mol}^{-1}$, respectively. It can be seen that the activation barrier of TS6 and TS10 is much higher than that of TS2 and TS4, which shows the reaction pathways forming products CO and H_2S are the most favorable in dynamics. Therefore, the pathway forming CO and H_2S is the major reaction, and the pathway producing CH₄ is a side reaction, which is in line with previous experimental findings very well [6, 8].

The rate constant for the reaction paths 2 and 3

As mentioned above, Paths 2 and 3 may be parallel reactions. To understand the reaction mechanism of H_2 with OCS at different temperature from the kinetic point of view, the activation thermodynamic parameters of the rate determining step in Paths 2 and 3 in the temperature range of 298.15~700 K and the corresponding rate constant have been calculated. The data are listed in Table 4. The change of activation thermodynamic properties is the difference between the activation thermodynamic data of transition state (TS2, TS4) and that of R2, R3 [13, 27, 28].

According to the activation entropy $\Delta_r^{\ddagger}S^\emptyset$ data in Table 4, it can be seen that these are entropy-decreasing pathways with increasing temperature. The activation free energy $\Delta_r^{\ddagger}G^\emptyset$ increases in the temperature range of 298.15~700 K. In the whole temperature range, it is the synthesis effect of the activation free energy together with the product of the activation entropy and temperature that causes the activation enthalpy $\Delta_r^{\ddagger}H^\emptyset$ to decrease slowly and monotonously with increasing temperature. This result shows that the activation enthalpy and free energy is an activation thermodynamic property which relates with temperature [29].

Finally, the rate constants for these two reaction pathways have been obtained using Eyring's transition state theory (TST) [30, 31]. From Table 4, it can be seen that the rate constant k increases rapidly with increasing temperature, but the increasing extent becomes small when the temperature is higher. At the same temperature, the rate constant of Path 2 is larger than that of Path 3, and this

Table 4 The activation enthalpy $\Delta_r^{\ddagger}H^\emptyset$ ($\text{kJ}\cdot\text{mol}^{-1}$), activation free energy $\Delta_r^{\ddagger}G^\emptyset$ ($\text{kJ}\cdot\text{mol}^{-1}$), activation entropy $\Delta_r^{\ddagger}S^\emptyset$ ($\text{J}\cdot\text{K}^{-1}\cdot\text{mol}^{-1}$), activation energy ($\text{kJ}\cdot\text{mol}^{-1}$), rate constant k ($\text{cm}^3\cdot\text{mol}^{-1}\cdot\text{K}^{-1}$) for Paths 2 and 3

	T(K)	$\Delta_r^{\ddagger}H^\emptyset$	$\Delta_r^{\ddagger}S^\emptyset$	$\Delta_r^{\ddagger}G^\emptyset$	E_a	k
Path 2	298.15	279.885	-26.568	287.807	282.364	2.34×10^{-38}
	500	279.233	-28.865	293.665	283.390	2.18×10^{-18}
	700	278.814	-29.434	299.418	284.634	6.61×10^{-10}
Path 3	298.15	291.374	-39.832	303.249	293.852	4.60×10^{-41}
	500	289.302	-45.396	312.001	293.459	2.64×10^{-20}
	700	289.235	-45.580	321.142	295.055	1.58×10^{-11}

sequence does not change with the temperature change, which implies that Path 2 is superior to Path 3. In addition, with the increasing temperature, especially in the high temperature, the competitive capacity of Path 3 increases, which means that when the reaction of Path 2 is occurring, a small reaction of Path 3 also occurs. Combining with the analysis of activation energy, we think that it is greatly reasonable for Path 2 existing in the form of the main reaction path to form the major products CO and H₂S. This computational result of kinetic reaction is the same as the experimental findings.

Conclusions

Density functional theory is used to explore the potential energy surface for the reaction of H₂ with OCS, and the detailed reaction mechanisms of H₂ with OCS are presented. Five intermediates and ten transition states are located along the reaction pathways. The calculated results show that the production of CO and H₂S is the major reaction pathway, which is consistent with the experimental results. And the main reaction pathway leading to the formation of CO and H₂S is that H atom of H₂ attacks the center C atom and end S atom in OCS.

Acknowledgments This work was supported financially by the National Basic Research Program of China (No. 2005CB221203), the National Natural Science Foundation of China (No. 20976115, 20776093 and 20906066), and the Foundation of Shanxi Province (No.2006011022).

References

1. Liu JF, Liu YC, Xue L, Yu YB, He H (2007) Acta Phys-Chim Sin 23:997–1002
2. Hodes RC, Riddel SA, West J, Williams BP, Hutchings GJ (2000) Catal Today 59:443–464
3. Watts SF, Roberts CN (1998) Atmos Environ 33:169–170
4. Pearson MJ (1981) Hydrocarbon Process 60:131–134
5. Williams BP, Young NC, West J, Rhodes C, Hutchings GJ (1999) Catal Today 49:99–104
6. Li XX, Liu YX, Wei XH (2004) Modern Chem Industry 24:19–22
7. Álvarez-Rodríguez R, Clemente-Jul C (2008) Fuel 87:3513–3521
8. Wang FF, Wu XL, Zhao H, Zhang DX (2007) Coal Chem Industry 130:28–32
9. Zhou ZY, Xing R, Shen WQ, Dou BL, Sha XZ (2003) Gas Heat 23:3–6
10. Yang T, Wen XD, Huo CF, Li YW, Wang JG, Jiao HJ (2009) J Mol Catal A: Chem 30:129–136
11. Rice BM, Cartland HE, Chabalowski GF (1993) Chem Phys Lett 211:283–292
12. Häusler D, Rice J, Wittig C (1987) J Phys Chem 91:5413–5415
13. Zhang WC, Du BN, Feng CJ (2005) J Mol Struct Theochem 726:25–30
14. Becke AD (1988) J Chem Phys 88:2547–2553
15. Lee C, Yang W, Parr RG (1988) Phys Rev B 37:785–789
16. Sauer J (1992) In: Catlow CRA (ed) Modeling of structure and reactivity in zeolites. Academic, London, pp 206–207
17. Zhang RG, Huang W, Wang BJ (2007) Chin J Catal 28:641–645
18. Delley B (1990) J Chem Phys 92:508–517
19. Delley B (2000) J Chem Phys 113:7756–7764
20. Gao LG, Song XL (2007) J Mol Struct Theochem 820:12–17
21. Luo YR (2005) Handbook of chemical bond dissociation energies. Science Press, Beijing
22. Pedley JB, Naylor RD, Kirby SP (1986) Thermochemical data of organic compounds. Chapman and Hall, London
23. Prinslow DA, Armentrout PB (1991) J Chem Phys 94:3563–3567
24. Lahaye JG, Vandenhaute R, Fayt A (1987) J Mol Spectrosc 123:48–83
25. Nicovich JM, Kreutter KD, van Dijk CA, Wine PH (1992) J Phys Chem 96:2518–2528
26. Ruscic B, Wagner AF, Harding LB, Asher RL, Feller D, Dixon DA, Peterson KA, Song Y, Qiam XX, Ng CY, Liu J, Chen W, Schwenke DW (2002) J Phys Chem A 106:2727–2747
27. Zhu KK, Wang YB, Huang MB, Wen ZY (2000) Acta Chim Sin 58:519–523
28. Si WJ, Gao SP, Ju GZ (2003) Acta Phys Chim Sin 19:974–977
29. Wang H, Yang HF, Ran XQ, Wen ZY, Shi QZ (2002) J Mol Struct Theochem 581:1–9
30. Fu XC, Shen WX, Yao TY (1990) Physical chemistry, 4th edn. Higher Education Press, Beijing, pp 798–812
31. Wang BJ, Wei XY, Xie KC (2004) Chin J Chem Eng 55:569–574